

Article

Modeling the Stress-Induced Transformation Behavior of Shape Memory Alloys under Multiaxial Loading Conditions

Lei Chen ¹, Hongying Zhang ^{1,2}, Mitao Song ¹, Xinxin Yue ³ and Jian Zhang ^{1,*} 

¹ Faculty of Civil Engineering & Mechanics, Jiangsu University, Zhenjiang 212013, China; chen1573@ujs.edu.cn (L.C.); hyzhang-2008@163.com (H.Z.); songmt2004@163.com (M.S.)

² School of Science, Harbin Institute of Technology, Shenzhen 518055, China

³ College of Architecture, Anhui Science and Technology University, Bengbu 233030, China; yuexinxin@ahstu.edu.cn

* Correspondence: jianzhang@ujs.edu.cn

Abstract: A large number of criteria to model the onset of plasticity for ductile metals have been proposed by researchers in the last century. Strangely, very few researchers have tried to model the stress-induced crystalline phase transformation of Shape Memory Alloys (SMAs) according to yield criteria. This paper focuses on the question: is a yield criterion originally proposed for describing the plastic behavior of metals suitable to model the “pseudoelastic” behavior of SMAs? To answer this question, two yield criteria originally proposed by the present author are used to predict the initial surface of transformation onset of two different SMAs: Cu-Al-Be and Ni-Ti alloy. The predicted initial transformation onset surfaces of the two SMAs are compared with experimental results and existing theories reported in the literature and some significant conclusions and recommendations are given.

Keywords: transformation condition; initial surface of transformation onset; martensite start surface; yield criterion; shape memory alloy



Citation: Chen, L.; Zhang, H.; Song, M.; Yue, X.; Zhang, J. Modeling the Stress-Induced Transformation Behavior of Shape Memory Alloys under Multiaxial Loading Conditions. *Crystals* **2021**, *11*, 1191. <https://doi.org/10.3390/cryst11101191>

Academic Editor: Sergio Brutti

Received: 28 August 2021

Accepted: 28 September 2021

Published: 30 September 2021

Publisher's Note: MDPI stays neutral with regard to jurisdictional claims in published maps and institutional affiliations.



Copyright: © 2021 by the authors. Licensee MDPI, Basel, Switzerland. This article is an open access article distributed under the terms and conditions of the Creative Commons Attribution (CC BY) license (<https://creativecommons.org/licenses/by/4.0/>).

1. Introduction

Shape memory alloy (SMA) is a new functional material that can change crystalline phase at certain temperatures and stress levels, i.e., the so-called martensitic transformation [1–3]. With unique characteristics such as the “shape memory effect” and “pseudoelastic” behavior, SMAs have been widely used in aeronautics and astronautics [4–6], robotics [7,8] and medical devices [9,10], etc. Some of the applications involve the design of a linear actuator for high cycle duty using the one-way shape memory effect in SMA springs [11–13]. For more information on the applications of SMAs, one may refer to Costanza and Tata [14] and Malik et al. [15]. In addition to the widespread application of martensitic strengthening in steel, martensitic transformation can also be used to control deformation and improve the properties of metals in heat treatment [15]. As the unique characteristics of SMAs are related to martensitic transformation, accurate and reliable prediction of the hysteresis response is especially important [16]. For better application of SMAs, the mechanical behavior of SMAs under multiaxial proportional and nonproportional loadings has been studied extensively by means of both experiments and macroscopic models [17–20]. On the other hand, the asymmetric transformation behavior of SMAs has also been studied in experiments and molecular dynamics simulations [21–23]. In order to promote the application of SMAs at high temperature, various studies tried to increase the transformation temperatures of SMAs by adding alloying elements [24–27].

The martensitic transformation in SMAs is generally driven in two ways: temperature changes or applied stresses [1]. The present paper focuses on the “pseudoelastic” behavior of SMAs, i.e., the stress-induced phase transformation under isothermal conditions. We try to model the stress-induced crystalline phase transformation onset of SMAs using

macroscopic models. As we know, the transformation onset surface of SMA is the boundary of the domain, inside of which the martensite phase transformation is not activated, while the yield surface is the boundary between elasticity and plasticity. However, both surfaces are boundaries of domain in stress space. Therefore, it is reasonable to describe similar models to them. In fact, the famous von Mises yield criterion was previously used to describe the crystalline phase transformation onset of SMAs [28]. In order to describe the plastic behavior of metallic materials, a large number of yield criteria have been proposed in the last century. Some of them are widely used in industrial applications, such as the famous Tresca [29] and von Mises criterion [30] for isotropic materials, and the anisotropic criteria proposed by Hill [31], Barlat et al. [32], Banabic et al. [33], Cazacu et al. [34] and Yoon et al. [35]. However, very few researchers have tried to model the initial surface of transformation onset of SMAs according to yield criteria. To this end, the present paper tries to model the “pseudoelastic” behavior of SMAs according to yield criteria originally proposed for describing the plastic behavior of metals, and goes a step further to answer the question: is a yield criterion originally proposed for describing the plastic behavior of metals suitable to model the “pseudoelastic” behavior of SMAs? In the following, two yield criteria for pressure-insensitive metals originally proposed by the present author will be introduced briefly.

2. Tension–Compression Asymmetric Yield Criteria

The present author [36] proposed an isotropic yield criterion that can model the yielding asymmetry of pressure-insensitive metals, hereafter called J_2 - J_3 criterion. Further, the isotropic J_2 - J_3 criterion is extended to orthotropy to take plastic anisotropy into account, hereafter called J_2^0 - J_3^0 criterion. The J_2 - J_3 criterion has not been applied to any materials, while the J_2^0 - J_3^0 criterion can describe the plastic anisotropy and yielding asymmetry of several metallic materials very well, showing excellent predictive ability and flexibility.

In order to model the “pseudoelastic” behavior of SMAs, the two yield criteria mentioned above were used to predict the initial surface of the phase transformation onset of SMAs. In the following, the two yield criteria are briefly introduced; for more details, please refer to reference [36].

The isotropic criterion can be expressed as:

$$f \equiv J_2^{5/2} - \alpha J_2 J_3 = \tau_Y^5 \quad (1)$$

Here, J_2 represents the second invariant of the stress deviator S , and $J_3 = tr(S^3/3)$ represents the third invariant of the stress deviator S (tr represents the trace operator $tr(A) = \sum_{k=1}^3 A_{kk}$); α is a parameter describing the tension–compression asymmetry of materials and τ_Y is the yield shear stress. The main advantage of the proposed criterion is that it leads to a good approximation of yield loci calculated by the Taylor–Bishop–Hill crystal plasticity model.

Suppose σ_t is the uniaxial tensile yield stress, then we can obtain

$$\sigma_t = \tau_Y \left(\frac{81\sqrt{3}}{9 - 2\sqrt{3}\alpha} \right)^{1/5} \quad (2)$$

Suppose σ_c is the yield stress in uniaxial compression such that

$$\sigma_c = \tau_Y \left(\frac{81\sqrt{3}}{9 + 2\sqrt{3}\alpha} \right)^{1/5} \quad (3)$$

Hence,

$$\alpha = \frac{3\sqrt{3}}{2} \left(\frac{\sigma_t^5 - \sigma_c^5}{\sigma_t^5 + \sigma_c^5} \right) \quad (4)$$

$$\text{For } \sigma_t > \sigma_c > 0 \Rightarrow \alpha \in (0, 3\sqrt{3}/2) \quad (5)$$

$$\text{For } 0 < \sigma_t < \sigma_c \Rightarrow \alpha \in (-3\sqrt{3}/2, 0) \quad (6)$$

For materials with equal tensile and compressive yield stresses, i.e., $\alpha = 0$, the von Mises yield criterion is recovered. For the yield criterion to be convex, α is limited to a given numerical range: $(-2.25, 2.25)$.

For a state of plane stress, the J_2 - J_3 criterion is simplified as

$$\left[\frac{1}{3} (\sigma_1^2 - \sigma_1\sigma_2 + \sigma_2^2) \right]^{5/2} - \frac{\alpha}{81} (\sigma_1^2 - \sigma_1\sigma_2 + \sigma_2^2) [2\sigma_1^3 + 2\sigma_2^3 - 3(\sigma_1 + \sigma_2)\sigma_1\sigma_2] = \tau_Y^5 \quad (7)$$

For any $\alpha \neq 0$, the yield locus of Equation (7) is a “triangle” with rounded corners. As a demonstration, Figure 1 shows the plane stress yield loci of Equation (7) obtained corresponding to $\sigma_t/\sigma_c = 4/5, 1, 6/5$, respectively. These ratios correspond to $\alpha = -1.316, 0$ (von Mises) and 1.108 , respectively.

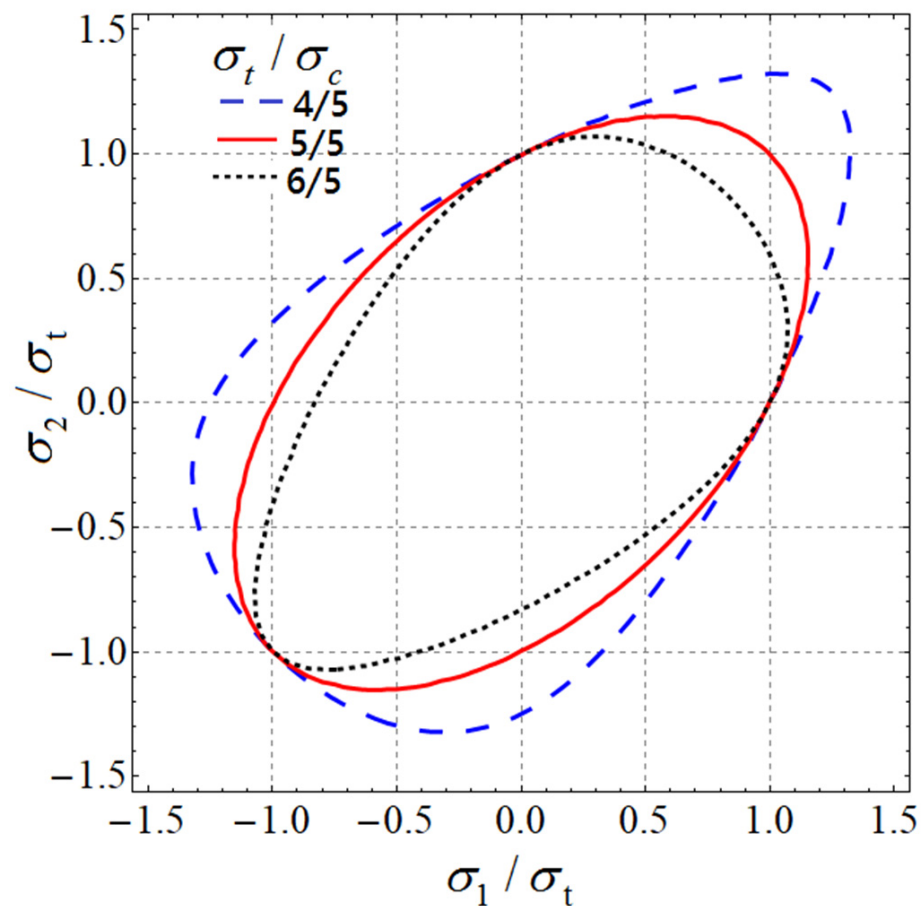


Figure 1. Yield loci predicted by the criterion (Equation (7)), according to $\sigma_t/\sigma_c = 4/5, 5/5$ (von Mises) and $6/5$.

In the (σ, τ) plane, the criterion is simplified as:

$$\left[\frac{1}{3} (\sigma^2 + 3\tau^2) \right]^{5/2} - \frac{\alpha}{81} (\sigma^2 + 3\tau^2) (2\sigma^3 + 9\tau^2\sigma) = \tau_Y^5 \quad (8)$$

where α can be determined by the yield stresses in pure shear and uniaxial tension according to the following relation:

$$\alpha = \frac{3\sqrt{3}}{2} - \frac{81}{2} \left(\frac{\tau_Y}{\sigma_t} \right)^5 \tag{9}$$

Figure 2 displays the yield loci in the tension–torsion plane (σ, τ) of the Tresca criterion, the proposed criterion (Equation (8)) according to $\sigma_t/\sigma_c = 4/5, 1$ (von Mises) and $6/5$, respectively. It can be seen that for $\sigma_t/\sigma_c \neq 1$, the yield locus of the proposed criterion departs sharply from that of the von Mises ellipse.

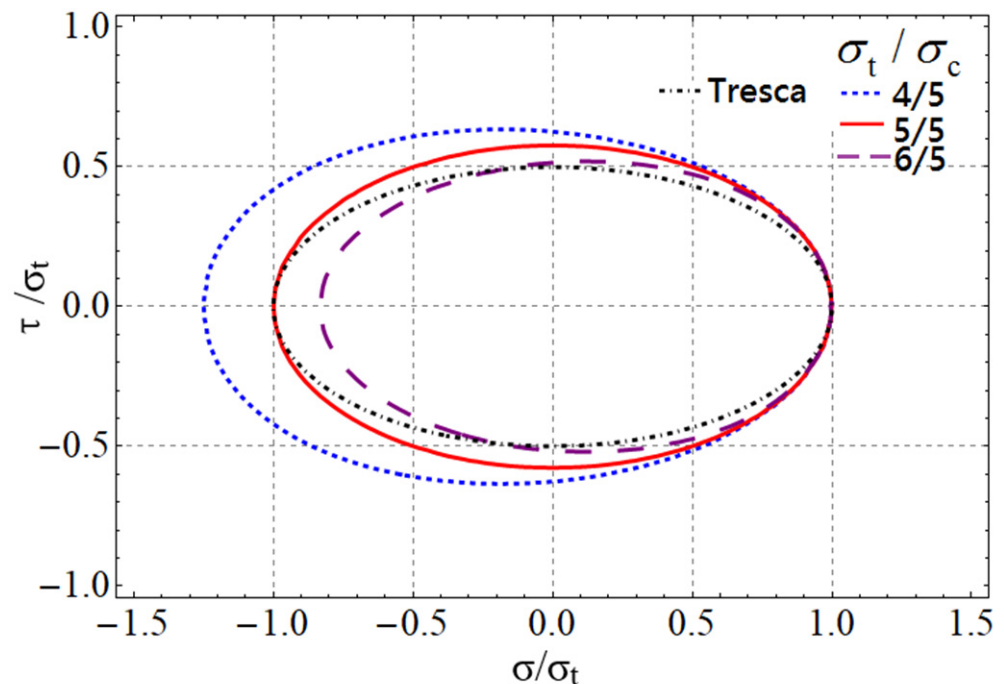


Figure 2. Yield loci predicted by the Tresca criterion and the isotropic yield criterion in the (σ, τ) plane for $\sigma_t/\sigma_c = 4/5, 5/5$ (von Mises) and $6/5$, respectively.

In order to take anisotropy into account, the criterion was extended by the orthotropic generalizations of the second and third invariant of the stress deviator, denoted by J_2^0 and J_3^0

$$\Phi \equiv \left(J_2^0 \right)^{5/2} - \alpha J_2^0 J_3^0 = \tau_Y^5 \tag{10}$$

where

$$J_2^0 = \frac{a_1}{6} (\sigma_{yy} - \sigma_{zz})^2 + \frac{a_2}{6} (\sigma_{zz} - \sigma_{xx})^2 + \frac{a_3}{6} (\sigma_{xx} - \sigma_{yy})^2 + a_4 \sigma_{yz}^2 + a_5 \sigma_{zx}^2 + a_6 \sigma_{xy}^2 \tag{11}$$

and

$$\begin{aligned} J_3^0 = & \frac{1}{27} (b_1 + b_2) \sigma_{xx}^3 + \frac{1}{27} (b_3 + b_4) \sigma_{yy}^3 + \frac{1}{27} [2(b_1 + b_4) - b_2 - b_3] \sigma_{zz}^3 \\ & - \frac{1}{9} (b_1 \sigma_{yy} + b_2 \sigma_{zz}) \sigma_{xx}^2 - \frac{1}{9} (b_3 \sigma_{zz} + b_4 \sigma_{xx}) \sigma_{yy}^2 - \frac{1}{9} [(b_1 - b_2 + b_4) \sigma_{xx} + (b_1 - b_3 + b_4) \sigma_{yy}] \sigma_{zz}^2 \\ & + \frac{2}{9} (b_1 + b_4) \sigma_{xx} \sigma_{yy} \sigma_{zz} - \frac{\sigma_{yz}^2}{3} [(b_6 + b_7) \sigma_{xx} - b_6 \sigma_{yy} - b_7 \sigma_{zz}] - \\ & \frac{\sigma_{zx}^2}{3} [2b_9 \sigma_{yy} - b_8 \sigma_{zz} - (2b_9 - b_8) \sigma_{xx}] - \frac{\sigma_{xy}^2}{3} [2b_{10} \sigma_{zz} - b_5 \sigma_{yy} - (2b_{10} - b_5) \sigma_{xx}] + 2b_{11} \sigma_{yz} \sigma_{zx} \sigma_{xy} \end{aligned} \tag{12}$$

For a thin sheet perpendicular to the z axis and in a condition of plane stress ($\sigma_{xx}, \sigma_{yy}, \sigma_{xy}$), the J_2 - J_3 criterion (Equation (10)) is expressed as

$$\Phi \equiv \left[\frac{1}{6}(a_1 + a_3)\sigma_{xx}^2 - \frac{a_1}{3}\sigma_{xx}\sigma_{yy} + \frac{1}{6}(a_1 + a_2)\sigma_{yy}^2 + a_4\tau_{xy}^2 \right]^{5/2} - \alpha \left[\frac{1}{6}(a_1 + a_3)\sigma_{xx}^2 - \frac{a_1}{3}\sigma_{xx}\sigma_{yy} + \frac{1}{6}(a_1 + a_2)\sigma_{yy}^2 + a_4\tau_{xy}^2 \right] \left\{ \begin{array}{l} \frac{1}{27}(b_1 + b_2)\sigma_{xx}^3 + \frac{1}{27}(b_3 + b_4)\sigma_{yy}^3 - \frac{1}{9}(b_1\sigma_{xx} + b_4\sigma_{yy})\sigma_{xx}\sigma_{yy} \\ -\frac{1}{3}\sigma_{xy}^2[(b_5 - 2b_{10})\sigma_{xx} - b_5\sigma_{yy}] \end{array} \right\} = \tau_Y^5 \quad (13)$$

In particular, the section of the yield locus with $\sigma_{xy} = 0$ is

$$\left[\frac{1}{6}(a_1 + a_3)\sigma_1^2 - \frac{a_1}{3}\sigma_1\sigma_2 + \frac{1}{6}(a_1 + a_2)\sigma_2^2 \right]^{5/2} - \alpha \left[\frac{1}{6}(a_1 + a_3)\sigma_1^2 - \frac{a_1}{3}\sigma_1\sigma_2 + \frac{1}{6}(a_1 + a_2)\sigma_2^2 \right] \left\{ \begin{array}{l} \frac{1}{27}(b_1 + b_2)\sigma_1^3 + \frac{1}{27}(b_3 + b_4)\sigma_2^3 - \frac{1}{9}(b_1\sigma_1 + b_4\sigma_2)\sigma_1\sigma_2 \end{array} \right\} = \tau_Y^5 \quad (14)$$

For the (σ, τ) stress state, the criterion becomes

$$\Phi \equiv \left[\frac{1}{6}(a_1 + a_3)\sigma^2 + a_4\tau^2 \right]^{5/2} - \alpha \left[\frac{1}{6}(a_1 + a_3)\sigma^2 + a_4\tau^2 \right] \left[\frac{1}{27}(b_1 + b_2)\sigma^3 - \frac{1}{3}(b_5 - 2b_{10})\sigma\tau^2 \right] = \tau_Y^5 \quad (15)$$

It is easy to prove that both the J_2 - J_3 criterion and the J_2^0 - J_3^0 criterion are insensitive to hydrostatic pressure, which are suitable to describe the phase transformation of SMAs. This is the case because SMA is considered to be pressure-insensitive alloy, whose phase transformation between austenite and martensite is accompanied with no volume change [17].

3. Applications

In order to check if the yield criteria originally proposed for describing the plastic behavior of metals are suitable to model the stress-induced initial transformation onset of SMAs, in the following, we will apply the J_2 - J_3 criterion and the J_2^0 - J_3^0 criterion to two different SMAs: Cu-Al-Be and Ni-Ti alloy.

For Cu-Al-Be SMA, the initial yield points of phase transformation initiation (austenite to martensite) were obtained by means of bi-compression tests on cubes and tension (compression)-internal pressure on tubes according to the method proposed by Bouvet et al. [16]. The experimental stresses of the initial transformation onset of Cu-Al-Be in the (σ_1, σ_2) plane at 35 °C are shown in Table 1 (data from Laydi and Lexcellent [37]).

Table 1. Experimental data of the initial transformation onset of Cu-Al-Be SMA at 35 °C (unit: MPa).

| i | 1 | 2 | 3 | 4 | 5 | 6 | 7 | 8 | 9 | 10 | 11 |
|------------|-------|-------|--------|-------|----|--------|---------|--------|--------|------|--------|
| σ_1 | 87.14 | 91.43 | 105.71 | 45.71 | 0 | -45.71 | -105.71 | -100 | -65.71 | 0 | 51.43 |
| σ_2 | 0 | 42.86 | 102.86 | 100 | 80 | 60 | 0 | -48.57 | -91.43 | -100 | -48.57 |

Figure 3 shows the experimental initial transformation onset surface of Cu-Al-Be SMA (experimental data is plotted with symbols). Note that the transformation onset surface of Cu-Al-Be SMA has a significant asymmetrical shape, and the compressive “yield” stress is 20% larger than the tensile “yield” stress. Figure 3 also shows the theoretical yield locus of the J_2 - J_3 criterion given by Equation (1). The parameter $\alpha = -1.1655$ was calculated by Equation (4) using experiment point 1 (87.14 MPa, 0) and experiment point 7 (-105.71 MPa, 0) from Table 1, and the shear strength τ_Y was calculated by Equation (3). For the sake of comparison, the yield surface of the von Mises criterion [26] is also plotted in Figure 3. Here $\sigma_t = 87.14$ MPa was chosen as the uniaxial yield strength in the von Mises criterion. From Figure 3, we can see that the J_2 - J_3 criterion fits the asymmetric transformation onset surface of Cu-Al-Be SMA quite well although some discrepancies between the predicted results and the experimental data were also found in some stress

states. Obviously, the discrepancies between the predicted results of the J_2 - J_3 criterion and the experimental data were caused by the slight anisotropic pseudoelastic behavior of Cu-Al-Be SMA. As the von Mises criterion is based on the hypothesis of tension–compression symmetry, it failed to reproduce the asymmetry shape of the transformation onset surface for Cu-Al-Be. Undoubtedly, modeling of the pseudoelastic behavior of SMAs with remarkable tension–compression asymmetry using symmetric yield criteria (such as the von Mises criterion) will cause significant errors.

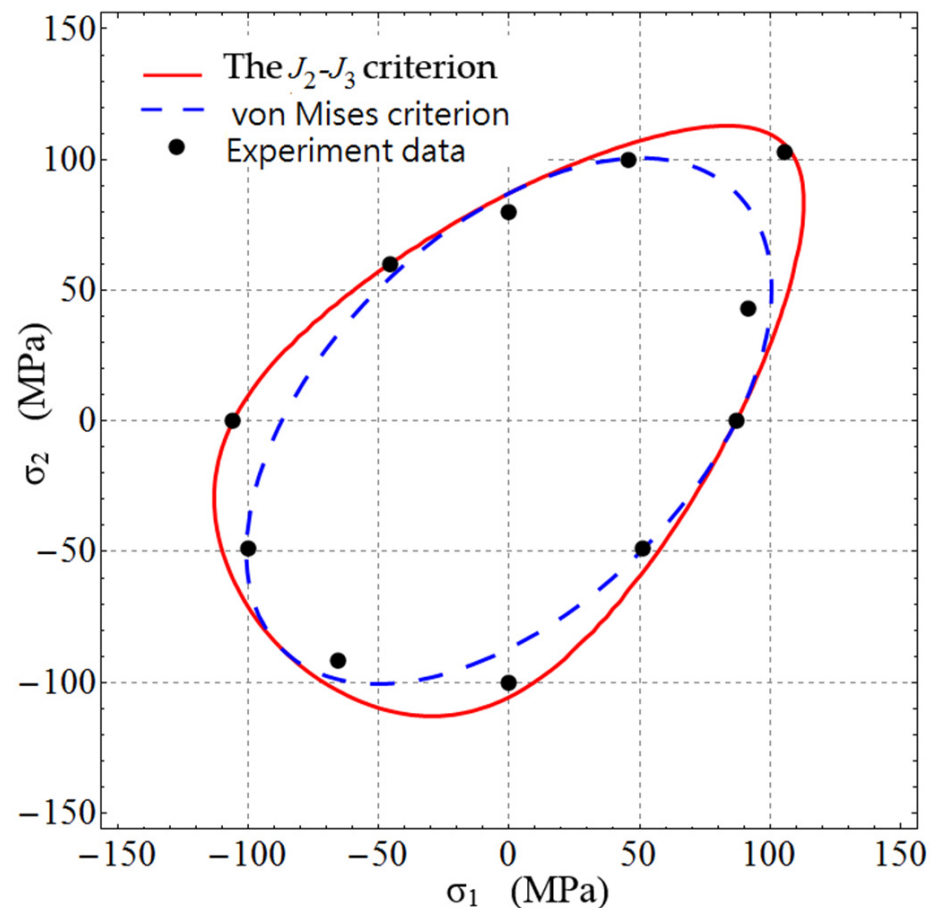


Figure 3. Comparison of experimental results and the theoretical initial transformation onset surfaces for Cu-Al-Be SMA in the (σ_1, σ_2) plane at 35 °C predicted by the J_2 - J_3 criterion and the von Mises criterion.

From the above analyses, the anisotropic pseudoelastic behavior of Cu-Al-Be SMA should be considered to obtain better prediction results. Figure 4a shows the comparison between the experimental results and the J_2^0 - J_3^0 criterion given by Equation (10), the parameters of which were calculated using the error minimization procedure (see Table 2). Clearly, the J_2^0 - J_3^0 criterion fits the experimental data better than J_2 - J_3 criterion. The J_2^0 - J_3^0 criterion can model the asymmetric transformation onset surface of Cu-Al-Be SMA very well except in the case of experiment point 2 (91.43 MPa, 42.86 MPa), which seems to be an experimental mistake. Therefore, anisotropic yield criterion with tension–compression asymmetry should be considered for precise modelling of the pseudoelastic behavior of such SMAs as Cu-Al-Be alloy.

Table 2. Anisotropic and tension–compression asymmetry parameters of the J_2^0 - J_3^0 criterion and the Cazacu–Barlat criterion for Cu–Al–Be SMA at 35 °C.

| Yield Criterion | a_1 | a_2 | a_3 | b_1 | b_2 | b_3 | b_4 | A |
|-----------------------------|--------|--------|--------|--------|--------|--------|--------|---------|
| Cazacu (2004) | 1.0509 | 1.3441 | 1.0261 | 0.7799 | 0.7173 | 0.9639 | 1.1559 | −1.6505 |
| J_2^0 - J_3^0 criterion | 1.0497 | 1.3070 | 1.0379 | 0.9256 | 0.8932 | 1.1147 | 1.2990 | −1.4713 |

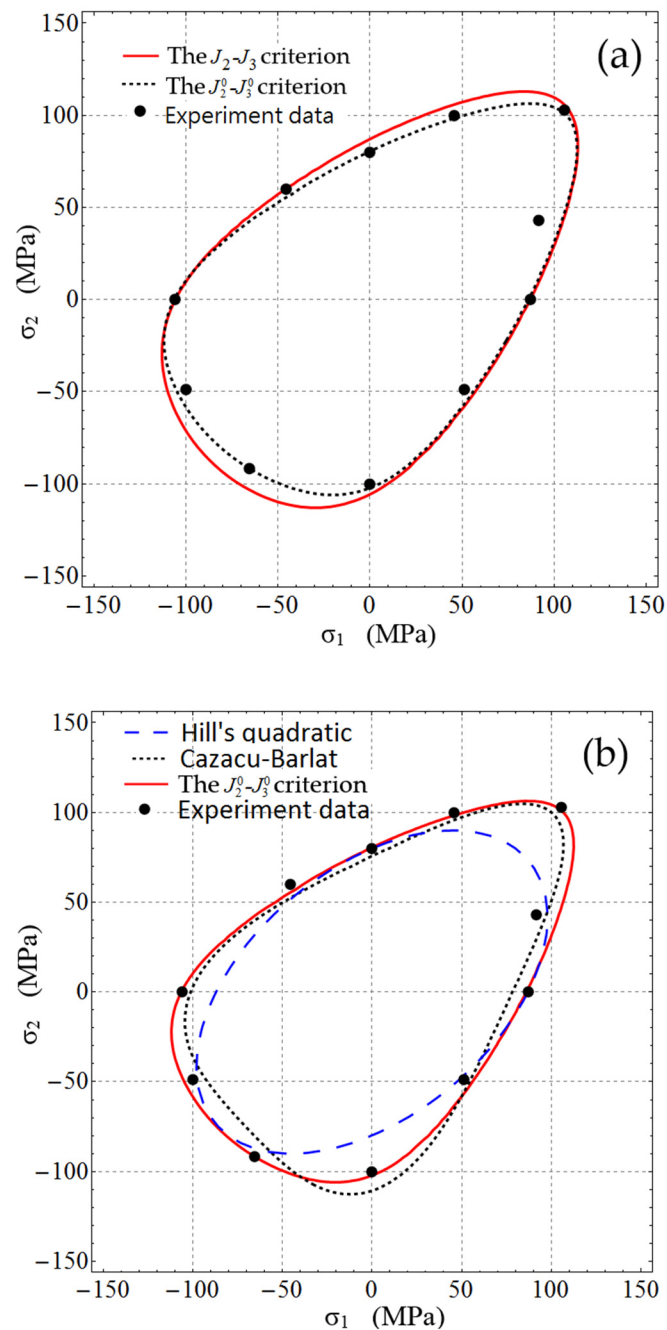


Figure 4. Comparison of experimental results and the theoretical initial transformation onset surfaces for Cu–Al–Be SMA in the (σ_1, σ_2) plane predicted by yield criteria: (a) the J_2 - J_3 criterion and the J_2^0 - J_3^0 criterion; (b) the J_2^0 - J_3^0 criterion, Hill's quadratic criterion and the Cazacu–Barlat criterion.

In order to compare the J_2^0 - J_3^0 criterion with existing theories in the literature, the yield locus of the J_2^0 - J_3^0 criterion, Hill's quadratic criterion [31] and the Cazacu–Barlat crite-

riterion [34] are plotted together in Figure 4b. The calculated parameters for Hill's quadratic criterion are given in Table 3. For Hill's quadratic criterion, significant discrepancies with experiment results were found for some stress states, especially for the equi-biaxial tension and uniaxial compression states. It should be mentioned that tensile transformation onset stresses were used here to calibrate the parameters of Hill's theory; therefore, the theoretical uniaxial compressive transformation onset stresses did not coincide with the experimental data. As Hill's quadratic criterion is based on the hypothesis of tension–compression symmetry, it failed to reproduce the asymmetry shape of the experimental transformation onset locus of Cu-Al-Be SMA.

Table 3. Calculated parameters of Hill's quadratic function for Cu-Al-Be SMA at 35 °C.

| <i>F</i> | <i>G</i> | <i>H</i> |
|------------------------|------------------------|------------------------|
| 9.019×10^{-5} | 6.606×10^{-5} | 6.606×10^{-5} |

The calculated parameters of the Cazacu–Barlat criterion are given in Table 2. The predicted transformation onset surface of Cu-Al-Be by the Cazacu–Barlat criterion had a similar shape as that of the J_2^0 - J_3^0 criterion. Both criteria could model the asymmetric pseudoelastic behavior of Cu-Al-Be SMA well. However, the Cazacu–Barlat criterion slightly undervalued the equi-biaxial tensile transformation onset stress, while the J_2^0 - J_3^0 criterion gave a better prediction.

As for Ni–Ti SMA, a series of two dimensional proportional and non-proportional, isothermal and non-isothermal experiments were conducted by Laverhne-Taillard et al. [38]. The shape of the initial transformation stress surface was determined at different temperatures. Table 4 shows the experimental data of the initial transformation onset for Ni–Ti SMA at 50 °C (data from Laydi and Lexcellent [37]). Table 5 shows the experimental data of the initial transformation onset for Ni–Ti SMA at –10 °C (data was estimated from the graph in Ref. [38])

Table 4. Experimental data of the initial transformation onset of Ni–Ti SMA at 50 °C (unit: MPa).

| <i>i</i> | 1 | 2 | 3 | 4 | 5 | 6 | 7 | 8 | 9 | 10 | 11 | 12 | 13 | 14 | 15 |
|----------|-----|-----|-----|-----|-----|------|------|------|------|------|------|------|------|------|------|
| σ | 400 | 390 | 310 | 220 | 0 | –210 | –370 | –520 | –530 | –520 | –430 | –200 | 30 | 250 | 370 |
| τ | 0 | 150 | 240 | 340 | 440 | 420 | 330 | 220 | 0 | –150 | –340 | –400 | –370 | –300 | –150 |

Table 5. Experimental data of the initial transformation onset of Ni–Ti SMA at –10 °C (unit: MPa).

| <i>i</i> | 1 | 2 | 3 | 4 | 5 | 6 | 7 | 8 | 9 | 10 | 11 |
|----------|----|----|----|----|----|-----|-----|-----|-----|-----|-----|
| σ | 25 | 22 | 12 | 15 | 0 | –17 | –27 | –38 | –40 | –3 | 18 |
| τ | 0 | 2 | 18 | 20 | 25 | 21 | 20 | 2 | 0 | –27 | –14 |

Figure 5 shows the experimental shape of the initial transformation onset surface of Ni–Ti SMA in the (σ , τ) plane at 50 °C (experimental data is plotted with symbols). Note that the transformation onset surface of Ni–Ti SMA has a significant asymmetrical shape, and the transformation onset stress in compression is about 30% larger than that in tension. Moreover, a very high level of the transformation onset stress in torsion was observed in Ni–Ti SMA (i.e., $\tau_y = 430$ MPa), which was larger than that in uniaxial tension ($\sigma_y^t = 400$ MPa). This phenomenon is almost impossible to find in the plastic behavior of common metallic materials. Actually, the von Mises criterion predicts that $\tau_y/\sigma_y^t = 1/\sqrt{3}$, while the Tresca criterion gives $\tau_y/\sigma_y^t = 0.5$ for isotropic metals. For an isotropic SMA,

Bouvet et al. [12] showed that the transformation onset stress in torsion, τ_y^{iso} , is related to the tensile yield stress σ_y^t and compressive yield stress σ_y^c by:

$$\tau_y^{iso} = \frac{\sigma_y^t}{\sqrt{3}} \frac{1}{\cos\left(\frac{\cos^{-1}(1-a)}{3}\right)} \quad (16)$$

where a is a material parameter reflecting the tension–compression asymmetry calculated by the following equation:

$$a = \frac{1 - \cos\left[3 \cos^{-1}\left(\frac{\sigma_y^t}{\sigma_y^c}\right)\right]}{2} \quad (17)$$

Substituting the experimental data from Table 4 to Equations (16) and (17), $a = 0.97$ and $\tau_y^{iso} = 282$ MPa were obtained for Ni–Ti SMA. For an isotropic SMA with tension–compression symmetry (i.e., $\sigma_y^t = \sigma_y^c$), $a = 0$ and $\tau_y^{iso} = \sigma_y^t / \sqrt{3}$ were obtained, which is consistent with the prediction of von Mises. The large difference between τ_y and τ_y^{iso} was due to the anisotropy of SMA.

In the following, we attempt to model the initial transformation onset of Ni–Ti SMA in the (σ, τ) plane. For the isotropic J_2 - J_3 criterion, the parameter α was calculated by Equation (9). Due to the high value of τ_y , a very large $\alpha = 55.545$ was obtained, which was outside of the interval $\alpha \in (-2.25, 2.25)$ to ensure the convexity of the criterion. Figure 5 shows the theoretical yield locus of the J_2 - J_3 criterion for Ni–Ti SMA. Undoubtedly, the initial transformation onset surface predicted by the J_2 - J_3 criterion was meaningless in this case. Therefore, isotropic criteria such as the J_2 - J_3 criterion in this paper were found to be inappropriate to model the stress-induced transformation behavior of such SMAs as Ni–Ti alloy. The yield loci of Tresca and von Mises are also plotted in Figure 5. The yield shear stress τ_y and tensile yield stress σ_y^t were used to calibrate both of the criteria shown in Figure 5a,b, respectively. The results show that both criteria failed to model the initial transformation onset surface of Ni–Ti SMA.

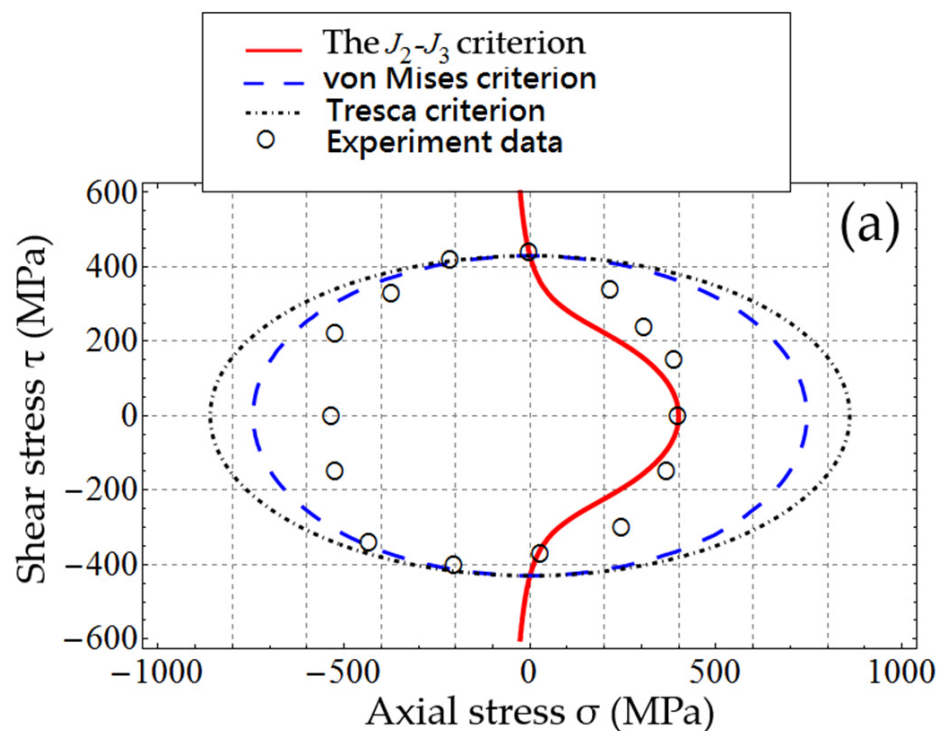


Figure 5. Cont.

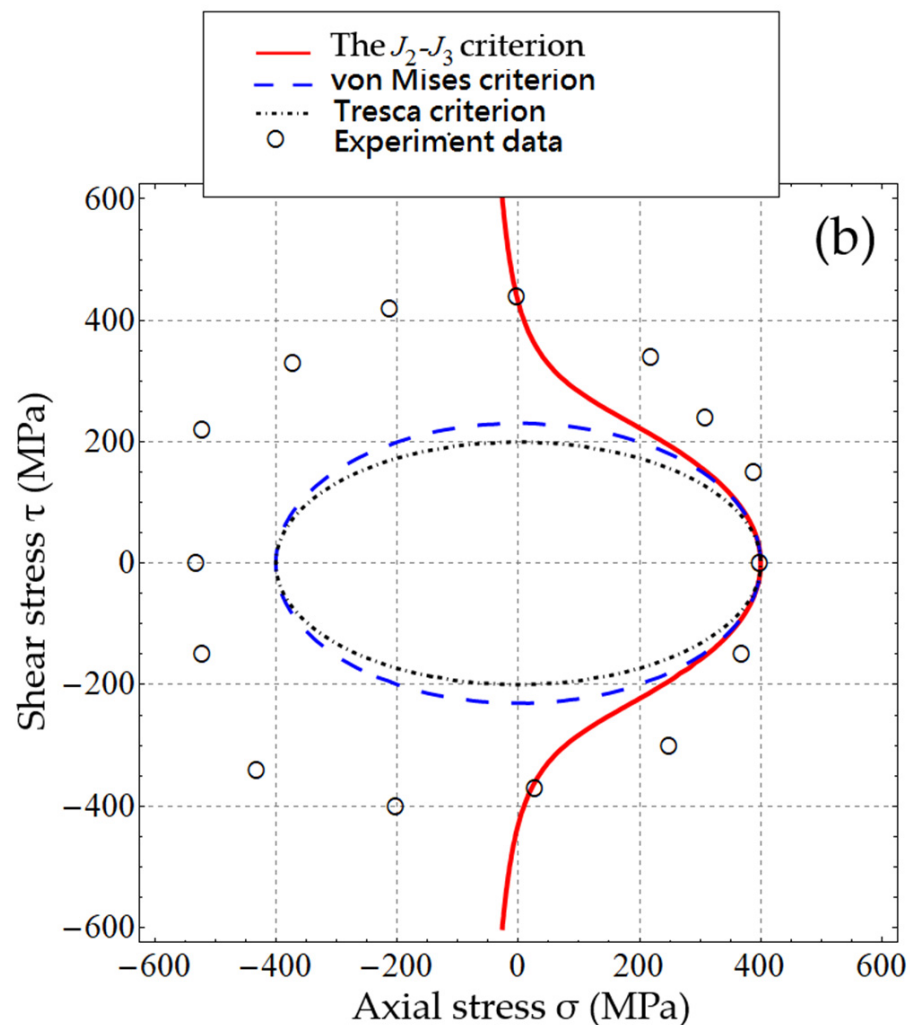


Figure 5. Comparison of experimental results and the theoretical initial transformation onset surfaces for Ni–Ti SMA in the (σ, τ) plane predicted by the criterion, the Tresca criterion and the von Mises criterion: (a) calibrated by τ_y ; (b) calibrated by σ_y^t .

As mentioned above, the large difference between τ_y and τ_y^{iso} is due to the anisotropy of SMA. The large ratio of $\tau_y / \tau_y^{iso} (=1.52)$ reflects a significant anisotropy of the stress-induced transformation behavior for Ni–Ti alloy at 50 °C. Therefore, to model the stress-induced transformation behavior of the Ni–Ti alloy precisely, the anisotropy of SMA must be considered. In the following, the anisotropic J_2^0 - J_3^0 criterion will be applied to model the initial transformation onset of Ni–Ti SMA in the (σ, τ) plane. In order to calibrate the anisotropy and tension–compression parameters of the criterion, the experimental data points in Table 3 ($i = 1, 2, 3, 4, 5, 7, 9, 11, 13, 15$) were adopted. The eight parameters of the J_2^0 - J_3^0 criterion in (σ, τ) plane (Equation (15)) were determined using the differential evolution algorithm [39,40] with the objective of minimal fit error to the experimental data. The calculated parameters are listed in Table 6. Figure 6a shows the comparison of experimental results and the J_2^0 - J_3^0 criterion of the initial transformation onset surface for Ni–Ti alloy in the (σ, τ) plane at 50 °C. The J_2^0 - J_3^0 criterion was able to give more effective results than those of the other three yield criteria; therefore, it could model the asymmetric transformation onset surface of Ni–Ti SMA very well.

For the −10 °C condition, similar results could be obtained. Table 7 shows the parameters of the J_2^0 - J_3^0 criterion for Ni–Ti SMA at −10 °C calculated using the same procedure as the 50 °C case. Figure 6b shows the experimental data and the predicted J_2^0 - J_3^0 criterion of the initial transformation onset surface for Ni–Ti alloy in the (σ, τ) plane at

−10 °C. Again, good correlation between the predicted initial transformation onset surface and the corresponding experimental data were obtained.

Furthermore, comparing the experimental surfaces of the phase transformation onset for Ni–Ti SMA at 50 °C and −10 °C, it is clear that not only the size, but also the shape, had changed. This phenomenon indicates that the characteristics of “pseudoelastic” behavior for Ni–Ti SMA changed from 50 °C to −10 °C. Therefore, it can be concluded that not only the scale parameter (i.e., τ_y), but also the anisotropic and asymmetric parameters of the criterion, should be adjusted accordingly. This point is well illustrated by the prediction results of the J_2^0 - J_3^0 criterion (see Figure 6 and the parameters of the criterion in Tables 6 and 7).

To this end, we may conclude that the J_2^0 - J_3^0 criterion is flexible enough to describe the stress-induced transformation onset of such SMAs as Cu–Al–Be and Ni–Ti alloys.

Table 6. Anisotropic and tension–compression asymmetry parameters of the J_2^0 - J_3^0 criterion for Ni–Ti SMA at 50 °C.

| a_1 | a_3 | a_4 | b_1 | b_2 | b_5 | b_{10} | α |
|--------|--------|--------|--------|--------|--------|----------|----------|
| 3.1975 | 2.5007 | 0.9551 | 6.1298 | 5.3587 | 1.0239 | 1.6285 | −1.3715 |

Table 7. Anisotropic and tension–compression asymmetry parameters of the J_2^0 - J_3^0 criterion for Ni–Ti SMA at −10 °C.

| a_1 | a_3 | a_4 | b_1 | b_2 | b_5 | b_{10} | α |
|--------|--------|--------|--------|--------|--------|----------|----------|
| 3.2965 | 2.3807 | 0.9862 | 9.5632 | 8.0192 | 1.6335 | 1.9263 | −1.2557 |

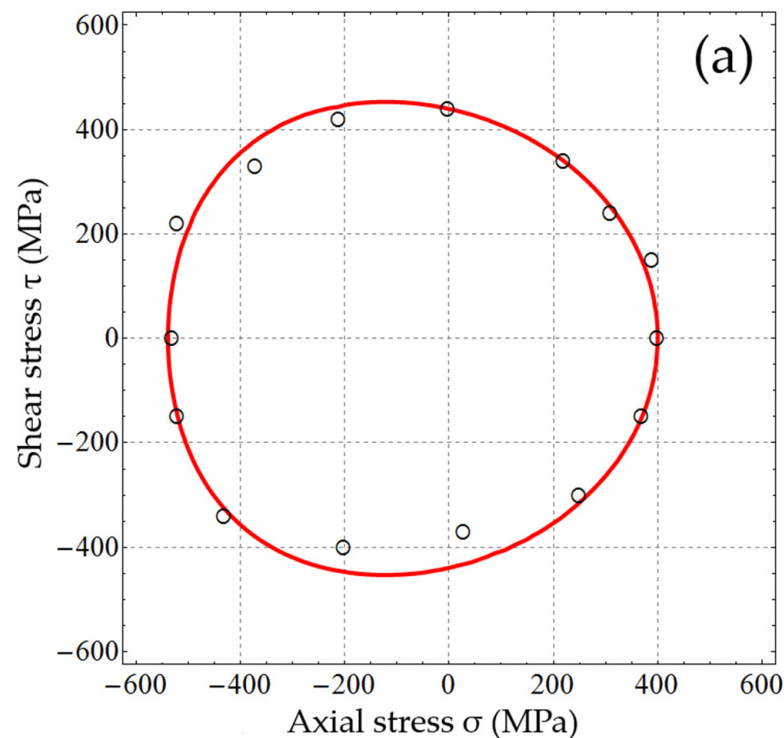


Figure 6. Cont.

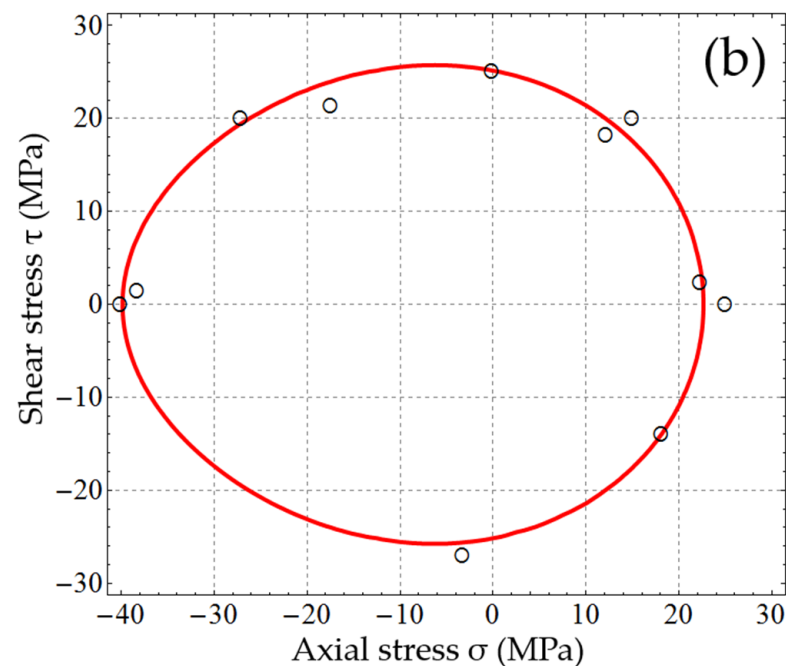


Figure 6. Comparison of experimental results (dots) and the theoretical initial transformation onset surface for Ni–Ti SMA in the (σ, τ) plane predicted by the J_2^0 - J_3^0 criterion (continuous line). (a): 50 °C; (b): −10 °C.

4. Conclusions

The isotropic J_2 - J_3 yield criterion and anisotropic J_2^0 - J_3^0 yield criterion originally proposed to model the plastic behavior of metals were applied to model the “pseudoelastic” behavior of SMAs. Both criteria considered the asymmetry between tension and compression. The primary focus in this paper was to model the stress-induced transformation behavior of SMAs. The initial transformation onset surfaces of two different SMAs under multiaxial loading conditions were modeled by both the J_2 - J_3 criterion and the J_2^0 - J_3^0 criterion. To precisely model the phase transformation surface of SMAs using the macroscopic model, further research is still needed, especially for the inverse transformation (martensite to austenite). For now, we can reach the following conclusions:

- (1) The yield criterion originally proposed for describing the plastic behavior of metals can be used to model the phase transformation surface of SMAs, but its predictive ability and flexibility should be checked carefully using experimental data.
- (2) The anisotropic J_2^0 - J_3^0 criterion originally proposed by the present author can model the asymmetric transformation onset surface of Cu–Al–Be and Ni–Ti SMA very well, and gives a better prediction compared to some existing theories in the literature.
- (3) The von Mises and Tresca criteria are not suitable to model the phase transformation surface of SMAs with remarkable asymmetric pseudoelastic behaviors between tension and compression.
- (4) To precisely model such SMAs as Ni–Ti alloy with significant tension–compression asymmetry and considerable difference between τ_y and τ_y^{iso} , anisotropy must be included in the yield criteria. As an example, the anisotropic J_2^0 - J_3^0 criterion originally proposed by the present author can model the asymmetric transformation onset surface of Ni–Ti SMA in the (σ, τ) plane very well, showing excellent predictive ability and flexibility.

In addition, it should be noted that the stress–strain curve modelling of SMAs is also very important, which is fundamental in the SMA’s applications as sensors or actuators. However, the discussion of these issues is beyond the scope of this article, and will be explored in our future work.

Author Contributions: Conceptualization, L.C. and J.Z.; methodology, L.C. and H.Z.; software, X.Y.; validation, L.C., H.Z. and M.S.; formal analysis, X.Y. and M.S.; investigation, L.C.; resources, L.C.; data curation, L.C.; writing—original draft preparation, L.C.; writing—review and editing, J.Z.; visualization, M.S.; supervision, J.Z.; project administration, J.Z.; funding acquisition, H.Z., M.S. and J.Z. All authors have read and agreed to the published version of the manuscript.

Funding: This research was funded by the National Natural Science Foundation of China (Grant No. 11872190, 11802106), the Natural Science Foundation of Jiangsu Province (Grant No. BK20170521, BK20201414) and the Research Foundation for Advanced Talents of Jiangsu University (Grant No. 16JDG050).

Data Availability Statement: All data, models, or code that support the findings of this study are available from the corresponding author upon reasonable request.

Conflicts of Interest: The authors declare no conflict of interest.

References

1. Huo, Y.; Müller, I. Nonequilibrium thermodynamics of pseudoelasticity, continuum mech. *Thermodynamics* **1993**, *5*, 163–204.
2. Bhattacharyya, A.; Lagoudas, D.; Wang, Y.; Kinra, V.K. On the role of thermoelectric heat transfer in the design of SMA actuators: Theoretical modeling and experiment. *Smart Mater. Struct.* **1995**, *4*, 252–263. [[CrossRef](#)]
3. Shaw, J.; Kyriakides, S. On the nucleation and propagation of phase transformation fronts in a NiTi alloy. *Acta Mater.* **1997**, *45*, 683–700. [[CrossRef](#)]
4. Coutu, D.; Brailovski, V.; Terriault, P. Optimized design of an active extradors structure for an experimental morphing laminar wing. *Aerosp. Sci. Technol.* **2010**, *14*, 451–458. [[CrossRef](#)]
5. Bashir, M.; Rajendram, P.; Sharma, C.; Smrutiranjana, D. Investigation of smart material actuators & aerodynamic optimization of morphing wing. *Mater. Today Proc.* **2018**, *5*, 21069–21075.
6. Chen, Y.; Shen, X.; Li, J.; Chen, J. Nonlinear hysteresis identification and compensation based on the discrete Preisach model of an aircraft morphing wing device manipulated by an SMA actuator. *Chin. J. Aeronaut.* **2019**, *32*, 1040–1050. [[CrossRef](#)]
7. Modabberifar, M.; Spenko, M. A shape memory alloy-actuated gecko-inspired robotic gripper. *Sens. Actuators A Phys.* **2018**, *276*, 76–82. [[CrossRef](#)]
8. Mohan, M.S.; Kumar, P.R.; Thirumalaikumarana, S.; Thanish, S. Impact of Cu-Al-Ni shape memory alloy in dynamic performance of redundant SCARA robot. *Mater. Today Proc.* **2020**, *28*, 776–780. [[CrossRef](#)]
9. Taniguchi, H. Flexible artificial muscle actuator using coiled shape memory alloy wires. *APCBEE Procedia* **2013**, *7*, 54–59. [[CrossRef](#)]
10. Sharma, N.; Gupta, K. Wire spark erosion machining of Ni rich niti shape memory alloy for bio-medical applications. *Procedia Manuf.* **2019**, *35*, 401–406. [[CrossRef](#)]
11. Costanza, G.; Tata, M.E.; Calisti, C. Nitinol one-way shape memory springs: Thermomechanical characterization and actuator design. *Sens. Actuators A Phys.* **2010**, *157*, 113–117. [[CrossRef](#)]
12. Costanza, G.; Paoloni, S.; Tata, M.E. IR thermography and resistivity investigations on Ni-ti shape memory alloy. *Key Eng. Mater.* **2014**, *605*, 23–26. [[CrossRef](#)]
13. Devashena, T.; Dhanalakshmi, K. Simultaneous measurements for the interlink of electro-thermo-mechano-electro characteristics in shape memory springs. *ISA Trans.* **2021**, in press. [[CrossRef](#)]
14. Costanza, G.; Tata, M.E. Shape memory alloys for aerospace, recent developments, and new applications: A short review. *Materials* **2020**, *13*, 1856. [[CrossRef](#)] [[PubMed](#)]
15. Malik, V.; Srivastava, S.; Gupta, S.; Sharma, V.; Vishnoi, M.; Mamatha, T. A novel review on shape memory alloy and their applications in extraterrestrial roving missions. *Mater. Today Proc.* **2021**, *44*, 4961–4965. [[CrossRef](#)]
16. Bouvet, C.; Calloch, S.; LExcellent, C. Mechanical behavior of a Cu-Al-Be shape memory alloy under multiaxial proportional and nonproportional loadings. *Trans. ASME* **2002**, *124*, 112–124.
17. Raniecki, B.; LExcellent, C. Thermodynamics of isotropic pseudoelasticity in shape memory alloys. *Eur. J. Mech. A/Solids* **1998**, *17*, 185–205. [[CrossRef](#)]
18. LExcellent, C.; Vivet, A.; Bouvet, C.; Calloch, S.; Blanc, P. Experimental and numerical determinations of the initial surface of phase transformation under biaxial loading in some polycrystalline shape-memory alloys. *J. Mech. Phys. Solids* **2002**, *50*, 2717–2735. [[CrossRef](#)]
19. Xiao, H. An explicit, straightforward approach to modeling SMA pseudoelastic hysteresis. *Int. J. Plast.* **2014**, *53*, 228–240. [[CrossRef](#)]
20. Wang, X.; Yao, X.; Schryvers, D.; Verlinden, B.; Wang, G.; Zhao, G.; Van Humbeeck, J.; Kustov, S. Anomalous stress-strain behavior of NiTi shape memory alloy close to the border of superelastic window. *Scr. Mater.* **2021**, *204*, 114135. [[CrossRef](#)]
21. Elibol, C.; Wagner, M.-X. Investigation of the stress-induced martensitic transformation in pseudoelastic NiTi under uniaxial tension, compression and compression–shear. *Mater. Sci. Eng. A Struct.* **2015**, *621*, 76–81. [[CrossRef](#)]

22. Wei, K.; Peng, Y.; Qu, Z.; Pei, Y.; Fang, D. A cellular metastructure incorporating coupled negative thermal expansion and negative Poisson's ratio. *Int. J. Solid. Struct.* **2018**, *150*, 255–267. [[CrossRef](#)]
23. Chen, X.; Chen, W.; Ma, Y.; Zhao, Y.; Deng, C.; Peng, X.; Fu, T. Tension-Compression asymmetry of single-crystalline and nanocrystalline NiTi shape memory alloy: An atomic scale study. *Mech. Mater.* **2020**, *145*, 103402. [[CrossRef](#)]
24. Firstov, G.; Kosorukova, T.; Koval, Y.; Odnosum, V. High entropy shape memory alloys. *Mater. Today Proc.* **2015**, *2*, S499–S503. [[CrossRef](#)]
25. Li, S.; Cong, D.; Sun, X.; Zhang, Y.; Chen, Z.; Nie, Z.; Li, F.Q.; Ren, Y.; Wang, Y.D. Wide temperature-range perfect superelasticity and giant elastocaloric effect in a high entropy alloy. *Mater. Res. Lett.* **2019**, *7*, 482–489. [[CrossRef](#)]
26. Piorunek, D.; Frenzel, J.; Jöns, N.; Somsen, C.; Eggeler, G. Chemical complexity, microstructure and martensitic transformation in high entropy shape memory alloys. *Intermetallics* **2020**, *122*, 106792. [[CrossRef](#)]
27. Chang, S.-H.; Kao, W.-P.; Hsiao, K.-Y.; Yeh, J.-W.; Lu, M.-Y.; Tsai, C.-W. High-temperature shape memory properties of Cu₁₅Ni₃₅Ti₂₅Hf_{12.5}Zr_{12.5} high-entropy alloy. *J. Mater. Res. Technol.* **2021**, *14*, 1235–1242. [[CrossRef](#)]
28. Raniecki, B.; Tanaka, K.; Ziolkowski, A. Testing and modeling of NiTi SMA at complex stress state. *Mater. Sci. Res. Int.* **2001**, *2*, 327–334.
29. Tresca, H. On the yield of solids at high pressures. *C. R. Acad. Sci.* **1864**, *59*, 754–758.
30. Mises, R. Mechanics of solid bodies in the plastically-deformable state. *Göttinger Nachr. Math. Phys.* **1913**, *1*, 582–592.
31. Hill, R. A theory of the yielding and plastic flow of anisotropic metals. *Proc. R. Soc. Lond. Ser. A Math. Phys. Sci.* **1948**, *193*, 281–297. [[CrossRef](#)]
32. Barlat, F.; Lege, D.J.; Brem, J.C. A six-component yield function for anisotropic materials. *Int. J. Plast.* **1991**, *7*, 693–712. [[CrossRef](#)]
33. Banabic, D.; Kuwabara, T.; Balan, T.; Comsa, D. An anisotropic yield criterion for sheet metals. *J. Mater. Process. Technol.* **2004**, *157–158*, 462–465. [[CrossRef](#)]
34. Cazacu, O.; Barlat, F. A criterion for description of anisotropy and yield differential effects in pressure-insensitive metals. *Int. J. Plast.* **2004**, *20*, 2027–2045. [[CrossRef](#)]
35. Yoon, J.W.; Lou, Y.S.; Yoon, J.H.; Glazoff, M.V. Asymmetric yield function based on the stress invariants for pressure sensitive metals. *Int. J. Plast.* **2014**, *56*, 184–202. [[CrossRef](#)]
36. Chen, L.; Zhang, J.; Zhang, H.J. Anisotropic yield criterion for metals exhibiting tension–compression asymmetry. *Adv. Appl. Math. Mech.* **2021**, *13*, 701–723.
37. Laydi, M.R.; LExcellent, C. Yield criteria for shape memory materials: Convexity conditions and surface transport. *Math. Mech. Solids* **2008**, *15*, 165–208. [[CrossRef](#)]
38. Lavernhe-Taillard, K.; Calloch, S.; Arbab-Chirani, S.; LExcellent, C. Multiaxial shape memory effect and superelasticity. *Strain* **2009**, *45*, 77–84. [[CrossRef](#)]
39. Zhou, H.Y.; Zhang, G.C.; Wang, X.J.; Ni, P.H.; Zhang, J. A hybrid identification method on butterfly optimization and differential evolution algorithm. *Smart Struct. Syst.* **2020**, *26*, 345–360.
40. Zhang, J.; Yue, X.; Qiu, J.; Zhang, M.; Wang, X. A unified ensemble of surrogates with global and local measures for global metamodelling. *Eng. Optim.* **2021**, *53*, 474–495. [[CrossRef](#)]